Tellus
SERIES A
DYNAMIC
METEOROLOGY
AND OCEANOGRAPHY
PUBLISHED BY THE INTERNATIONAL METEOROLOGICAL INSTITUTE IN STOCKHOLM

Tellus (2011), 63A, 41–55

TELLUS

Evaluation and future projections of temperature, precipitation and wind extremes over Europe in an ensemble of regional climate simulations

By GRIGORY NIKULIN*, ERIK KJELLSTRÖM, ULF HANSSON, GUSTAV STRANDBERG and ANDERS ULLERSTIG, *Rossby Centre, SMHI, SE 60196 Norrköping, Sweden*

(Manuscript received 28 October 2009; in final form 28 April 2010)

ABSTRACT

Temperature, precipitation and wind extremes over Europe are examined in an ensemble of RCA3 regional climate model simulations driven by six different global climate models (ECHAM5, CCSM3, HadCM3, CNRM, BCM and IPSL) under the SRES A1B emission scenario. The extremes are expressed in terms of the 20-yr return values of annual temperature and wind extremes and seasonal precipitation extremes.

The ensemble shows reduction of recurrence time of warm extremes from 20 yr in 1961–1990 (CTL) to 1–2 yr over southern Europe and to 5 yr over Scandinavia in 2071–2100 (SCN) while cold extremes, defined for CTL, almost disappear in the future. The recurrence time of intense precipitation reduces from 20 yr in CTL to 6–10 yr in SCN over northern and central Europe in summer and even more to 2–4 yr in Scandinavia in winter. The projected changes in wind extremes have a large spread among the six simulations with a disperse tendency (1–2 m s^{-1}) of strengthening north of 45°N and weakening south of it which is sensitive to the number of simulations in the ensemble. Changes in temperature extremes are more robust compared to those in precipitation extremes while there is less confidence on changes in wind extremes.

1. Introduction

Future climate scenarios show not only possible changes in the mean climate of the Earth system but also changes in extreme weather and climate events. Occurring on time scales from tens of minutes to seasons and longer extreme weather and climate events influence many aspects of human society: economy, ecosystem and health. Possible future changes in intensity and/or frequency of extreme events need new adaptation and risk management strategies taking into account how the statistics of extreme events may change. The primary tool providing information for developing such adaptation strategies is climate models simulating quantitatively climate changes under various future scenarios.

In the recent decade many investigations evaluated and documented statistics of observed (Trenberth et al., 2007; Gutowski et al., 2008) and simulated (Christensen et al., 2007; Kunkel et al., 2008) extreme events from both global (GCM) and regional (RCM) climate models. The most common three variables describing a wide range of extreme events are temperature, precipitation and wind.

On the global scale the future simulated warm and cold extremes show warming where warm extremes approximately follow the corresponding mean temperature of the warmest month of the year while cold extremes substantially exceed changes in the mean temperature of the coldest month of the year (Kharin and Zwiers, 2004; Kharin et al., 2007). The largest changes in warm extremes are generally confined to land areas, where there is a reduction in soil moisture, while the strongest reduction of cold extremes is confined to regions where snow and sea ice retreat by the global warming. Regional climate simulations over Europe have revealed the largest future warming in southern Europe for warm extremes that is related to soil moisture deficit in summer and in northern Europe for cold extremes as a response to reduced snow and ice cover in winter (Goubanova and Li, 2007; Kjellström et al., 2007). Moreover, the simulated changes in both cold and warm temperature extremes are larger then the corresponding changes in the mean suggesting also changes in temperature variability (Kjellström, 2004; Schär et al., 2004; Rowell, 2005; Fischer and Schär, 2009).

The projected intensity of precipitation extremes from GCMs increases almost everywhere over the world, even over regions with a decrease in mean precipitation, and generally exceeding

*Corresponding author.
e-mail: grigory.nikulin@smhi.se
DOI: 10.1111/j.1600-0870.2010.00466.x

those for mean precipitation (Kharin and Zwiers, 2004; Kharin et al., 2007). The simulated future changes in European precipitation extremes have a distinct seasonal pattern. In winter there is an increase north of about 45°N and smaller changes with tendency to a decrease to the south, while in summer a gradient from increases in Scandinavia to decreases in the Mediterranean region is evident (Christensen and Christensen, 2003; Kjellström, 2004; Räisänen et al., 2004; Frei et al., 2006; Beniston et al., 2007; Goubanova and Li, 2007). Wintertime projections of intense precipitation are consistent among different RCMs driven by one GCMs (Frei et al., 2006) and between simulations with one RCM driven by different GCMs (Räisänen et al., 2004). At the same time the summertime projections of precipitation extremes have more complex, mixed structure since the transition from north to south differs among RCMs and the magnitude of the change strongly depends on RCM physical parametrizations (Frei et al., 2006).

For maximum wind speeds over Europe RCM studies show a general tendency to stronger and more frequent extreme winds in the end of the century but there are very large discrepancies in magnitude, frequency and spatial patterns of the change among models which critically depend on how the driving GCMs simulate future changes in the large-scale circulation over the North Atlantic/European domain (Räisänen et al., 2003; Leckebusch et al., 2006; Beniston et al., 2007; Rockel and Woth, 2007). Another source of uncertainty is the method for calculating maximum daily wind speed which differs among RCMs since RCMs without gust parametrization are not able to realistically capture high wind speeds (Rockel and Woth, 2007).

In dynamical downscaling initial and lateral boundary conditions from driving GCMs play a major role defining the behaviour of corresponding RCM simulations (Déqué et al., 2007). At the same time the degree of influence of driving GCMs on the RCM results may depend on variable and season. In this study, we evaluate extremes of temperature, precipitation and wind over Europe and project their possible future changes applying an ensemble of integrations with one RCM driven by six different GCMs. Such an ensemble of six members allows us to estimate uncertainties in regional modelling related to driving GCMs and more specifically the degree of dependency of the simulated temperature, precipitation and wind extremes on driving GCMs.

2. Data and method

2.1. Model simulations

The downscaling of GCM simulations has been performed with the Rossby Center Regional Climate Model (RCA3) (Kjellström et al., 2005; Samuelsson et al., 2011). The RCA3 has a horizontal resolution of 0.44° (approximately 49 km) in a rotated latitude-longitude grid. The vertical discretization is in terms of vertical sigma-pressure coordinates with 24 levels (about 19 levels in the troposphere) and the upper boundary at near 10 hPa. The integration domain covers Europe and has 85 grid points in longitude and 95 in latitude excluding relaxation zones (Fig. 1). The regional simulations are driven by boundary conditions from the ERA40 reanalysis and six different GCMs: ECHAM5 (MPI, Germany), CCSM3 (NCAR, USA), HadCM3 (Hadley Center, UK), CNRM (CNRM, France), BCM (NERSC, Norway) and IPSL (IPSL, France) (for details see Kjellström et al., 2011). All simulations have employed the SRES-A1B emission scenario (Nakićenović et al., 2000) and two periods are chosen to represent the control (1961–1990, CTL) and possible future (2071–2100, SCN) climate.

For analysis we use daily maximum (T_{max}) and minimum (T_{min}) 2-m temperature, daily accumulated precipitation (P) and 10-m daily maximum gust wind (W_{max}). In the model, at each 30-min time step, the diagnostic variable 2-m temperature is calculated applying Monin–Obukhov similarity theory, individually for each tile (forest, open land and snow) and then averaged for the whole grid box (Samuelsson et al., 2006). The gust wind is estimated by a method of Brasseur (2001) using average roughness of grid boxes and additionally corrected to suppress overstimulation of wind gusts over land that occurs especially during storms (Nordström, 2005). The T_{max}, T_{min} and W_{max} parameters are simply defined as maximum or minimum values from all integrated time steps per day.

2.2. Observations

The simulated results for T_{max}, T_{min} and P and for the CTL period are validated against a daily high-resolution gridded observational data set for Europe (E-OBS) (Haylock et al., 2008). The E-OBS data set is based on point observations interpolated on the same rotated grid that is used in RCA3. Such a gridded observational data set, where each grid value is the best estimate average of the grid box observations rather than point values, enables appropriate evaluation of RCMs. In addition, to evaluate precipitation extremes, we also use the European Climate Assessment (ECA) observational data set (Klein Tank et al., 2002).

Unfortunately there is no consistent gridded data set for W_{max} since large spatial inhomogeneities of the W_{max} field together with sparse and/or short time series of observations preclude interpolation of W_{max} point observations to a grid in manner similar as for T_{max}, T_{min} and P. One available data set is an operational mesoscale analysis system—MESAN (Häggmark et al., 2000) that was used to evaluate W_{max} from RCA3 for 1999–2004 over Sweden (Kjellström et al., 2005). The agreement between RCA3 and MESAN for this period is quite satisfactory although RCA3 underestimates W_{max} around the big lakes in southern Sweden. Nevertheless, the MESAN data set covers only Sweden and is not long enough to evaluate wind extremes for our study. Another way is to validate the RCM results directly with observations taking the simulated W_{max} from the nearest grid

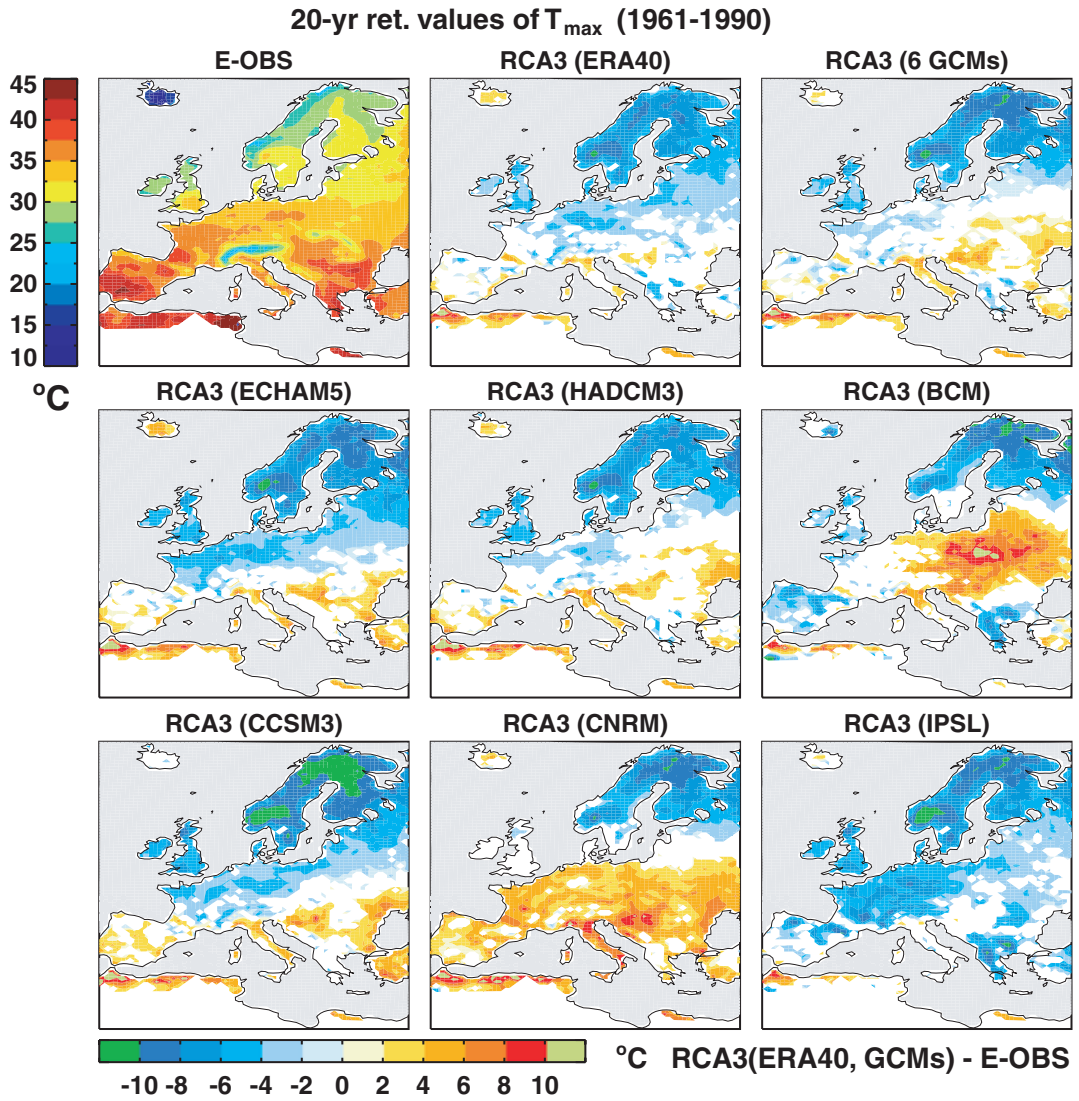

Fig. 1. $T_{\max,20}$ estimated from (top, left-hand panel) the E-OBS data and biases of $T_{\max,20}$ estimated from the RCA30 simulations driven by (top, middle panel) the ERA40 reanalysis, (middle and bottom rows) six different GCMs, (top, right-hand panel) their ensemble mean and with respect to the E-OBS (1961–1990). Units are °C. Only differences significant at the 10% significance level are shown.

point to observational stations (Leckebusch et al., 2006; Rockel and Woth, 2007). Such direct validation gives useful estimates of how well RCMs simulate gust wind locally but typically covers only a small part of the European domain and also results in inconsistency between the grid box average RCM and point observation gust wind. The quality of estimated gust wind in reanalyses that can be also potentially utilised for RCM validation is not good enough with, for example, unrealistic values over areas of complex topography in the ERA40 reanalysis (Della-Marta et al., 2007). Since there is no consistent data sets to evaluate quality of the RCA $W_{\max}$ for the whole European domain we focus only on possible future changes in the simulated wind extremes.

2.3. *Extreme value analysis*

To convey information about the statistics of rare events we use the extreme value analysis approach and express the estimated probabilities of extreme events in terms of T-year return values. The T-year return value is defined as the threshold that is exceeded any given year with the probability $1/T$ or, in a simplified interpretation, the threshold that is exceeded once every T years. The time T is referred to as the return period or waiting time. In order to estimate return values we apply the block maxima method (Coles, 2001) for which the generalised extreme value (GEV) distribution is the asymptotic distribution that describes the behaviour of block maxima with cumulative distribution

function

$$F(x,\mu,\sigma,\xi)=\begin{cases}\exp\left[-\exp\left(-\frac{x-\mu}{\sigma}\right)\right], & \xi=0\\ \exp\left[-\left(1+\xi\frac{x-\mu}{\sigma}\right)^{-\frac{1}{\xi}}\right], & \\ & \xi\neq 0,\ 1+\xi\frac{x-\mu}{\sigma}>0.\end{cases} \tag{1}$$

where x is the sampled maxima, μ is the location parameter, σ is the scale parameter (positive), and ξ is the shape parameter. The GEV distribution incorporates three types of distributions defined by the shape parameter ξ, namely: light-tailed Gumbel ($\xi = 0$), bounded Weibull ($\xi < 0$), and heavy-tailed Fréchet ($\xi > 0$) distributions. In climatological applications the block length n is typically chosen to be equal to 1 yr/season and the sampled extremes are the annual/seasonal maxima or minima in this case. We analyse annual extremes of $T_{\max}$, $T_{\min}$ and $W_{\max}$ and seasonal (summer and winter) extremes of P. After fitting the GEV distribution to the sampled extremes the T-year return values X_T are estimated by inverting the GEV cumulative distribution function (1):

$$X_T=\begin{cases}\mu-\sigma\ln\left[-\ln\left(1-\frac{1}{T}\right)\right], & \xi=0\\ \mu-\frac{\sigma}{\xi}\left[1-\left\{-\ln\left(1-\frac{1}{T}\right)\right\}^{-\xi}\right], & \xi\neq 0.\end{cases} \tag{2}$$

There are two common methods: L-moments (LMOM) (Hosking, 1990) and maximum likelihood (ML) (Coles, 2001) for fitting the GEV distribution to the annual extremes. The LMOM method is much more computationally efficient and also has better sampling properties in short samples for the shape parameter ξ comparing to the ML one (Hosking et al., 1985). The main disadvantage of the LMOM fitting is that the method only allows stationary models, assuming stationarity of the sampled annual extremes, that is, the GEV distribution parameters do not change with time. However, in transient climate simulations, when the greenhouse forcing gradually changes, the assumption of stationarity is not necessary valid. The ML method is more flexible in this sense since it allows to fit non-stationary models with linear and non-linear trends in the location, scale and shape parameters. A choice of an appropriate non-stationary model is straight forward for one grid point or area-average quantities using, for example, the standard deviance statistics to compare different statistical models (Coles, 2001). At the same time when we choose a non-stationary model for a large domain with several thousand grid points it is not a fact that the same statistical model can be applied to all grid points since the GEV distribution parameters may have different trends in different regions. Moreover, for an ensemble of different climate models, the main source of uncertainty in the estimated return values is intermodel spread which is much larger than uncertainy related to different methods (Kyselý, 2002; Kharin et al., 2007). The LMOM method is used here as the primary method for fitting of the GEV distribution, because of its simplicity and computational efficiency. In addition and to verify the results obtained with the LMOM fitting we also use the ML method with the three most common statistical models assuming: (i) stationary, (ii) a linear trend in the location and (iii) linear trends in both location and scale parameters For non-stationary models the estimated return values are calculated at the centre of the CTL and SCN periods. We have found no significant differences among the methods and therefore only results based on the LMOM method are presented here.

The Kolmogorov–Smirnov goodness-of-fit test is applied to check whether the sampled annual/seasonal extremes are realizations of a random process with the GEV distribution. Since the GEV distribution parameters are estimated from the data the critical values taken from statistical tables results in too conservative test, that is, the null hypothesis, that the sampled extremes are drawn from the GEV distribution, is rejected less frequently than indicated by the significance level (von Storch and Zwiers, 1999). More appropriate estimates of the critical value in this case are determined by a parametric bootstrap procedure (Kharin and Zwiers, 2000). For the temperature and wind extremes and for all simulations the number of grid points, where the null hypothesis is rejected, well corresponds to the 10% significant level chosen and no clustering of these grid points is evident. However, for the precipitation extremes the percentage of the rejected grid points over the whole domain is higher than can be expected from a random process. There are many clustering grid points in Africa with too small amount of precipitation in the CTL period and dryness of this region increases in the SCN period. Hence, we exclude all grid points located south of about 35°N from analysis of the precipitation extremes.

The statistical significance for the difference between the return values are determined by 500 parametric bootstraps of the original samples of $T_{\max}$, $T_{\min}$, P and $W_{\max}$. The return values are then calculated for each bootstrapped sample giving a family of the 500 surrogate estimates. We choose the 10% significance level that approximately corresponds to the non-overlapping 80% confidence intervals of two return level estimates (Kharin and Zwiers, 2004).

The same analysis as for the return levels is performed for the location, scale and shape parameters of the fitted GEV distribution but not shown because of large amount of visual materials and only shortly discussed.

3. Temperature extremes

3.1. Simulated temperature extremes in the control period

First of all we investigate how well the ensemble and its individual members reproduce the control climate. Figure 1 displays the 20-yr return values of $T_{\max}$ ($T_{\max,20}$) estimated from the gridded E-OBS data set for the CTL period and biases of the RCA3 simulations driven by the ERA40 reanalysis, by the six GCMs, and their ensemble mean with respect to the E-OBS. The $T_{\max,20}$

estimates from the E-OBS have the highest values, up to 45 °C, in northern Africa, the southern part of the Iberian and Balkan Peninsulas, decreasing northward, with typical values of about 35 °C in central Europe and about 25 °C in northern Scandinavia. The interpolation methodology of the E-OBS data set results in a reduced intensity of extremes hence local $T_{max,20}$ estimated directly from observations can be several degrees higher (Haylock et al., 2008).

A common feature, evident in all simulations in Fig. 1, is a large (up to 10 °C and more) underestimation of $T_{max,20}$ over Scandinavia. The annual maximum temperatures, sampled for the analysis, originate in summer season and a similar cold bias of the 95th percentile of summer daily T_{max} have been reported for 10 different RCMs driven by HadAM3H (Kjellström et al., 2007). The difference was possibly attributed to the HadAM3H boundary conditions. However, as we can see here, the same negative bias in Scandinavia also exists in the RCA3 runs driven by six different GCMs as well by the ERA40 reanalysis. The permanent cold bias in multiple simulations with different RCM and driving GCM combinations indicates that the representativity of the E-OBS data set on the RCM-scale (i.e. 2500 km^2) over Scandinavia in summer might be questionable. All observational stations are located on open land. The simulated T_{max}, on the other hand, is the grid box average, individually calculated for forests and open land areas. As maximum daytime temperature in summer is lower inside than outside of a forest this implies that the simulated T_{max} is lower than that observed in a region with a large forest fraction like Scandinavia.

This expectation could easily be verified by performing the same analysis for the open-land T_{max} but in the present configuration of RCA3 there is no the open-land T_{max} as a standard output parameter. The drawback has been fixed in next developing version—RCA35 and repeating the analysis for the RCA35 run driven by the ERA40 we found the same cold bias for the grid box average $T_{max,20}$ as for RCA3 but the bias is reduced by two to three times (within 0–4 °C) for the open-land $T_{max,20}$ (not shown). From this point of view the estimated $T_{max,20}$ from both simulated and observed annual T_{max} in Scandinavia are in good agreement and the inconsistency arises from the fact that the E-OBS data set represents only the open-land temperature.

Outside of Scandinavia, over continental Europe, the ERA40 driven run shows mixed biases with some tendency to underestimate $T_{max,20}$ in the north and overestimate it in the south. The bias pattern of $T_{max,20}$ over this region is disperse among six simulations driven by different GCMs. Three of them, RCA3(ECHAM5), RCA3(HadCM3) and RCA3(CCSM3) behave similar to the RCA3(ERA40) run showing some signs of a north–south dipole. The other three behave in different ways: RCA3(CNRM) overestimates $T_{max,20}$, RCA3(IPSL) underestimates, while RCA3(BCM) have a large overestimation in eastern Europe and an underestimation over the Iberian and Balkan Peninsulas. Corresponding biases in seasonal mean summer temperature (Kjellström et al., 2011, fig. 1) have a high degree of similarity to the ones in $T_{max,20}$: the coldest and warmest simulations are the same for mean and extreme temperatures. A detailed analysis of the fitted GEV parameters for each simulation reveals that the spatial patterns of the $T_{max,20}$ biases in Fig. 1 are similar to those of the location parameter, that is, biases in warm extremes are mainly due to a shift of the whole GEV distribution (not shown). In addition, the largest overestimation in the RCA3(BCM) and RCA3(CNRM) runs coincide with regions where the scale parameter of the fitted GEV distribution is about twice as large as the corresponding one for the E-OBS (not shown). Hence, the interannual variability of warm extremes over these regions is strongly overestimated in these two runs and biases in warm extremes are additionally amplified by a change in the shape of the GEV distribution. Overall, the wide spread of biases with different signs among the members of the ensemble south of 55°N results in an ensemble mean bias that is similar to the ERA40 driven run or even smaller.

The coldest extremes ($T_{min,20}$) estimated from the E-OBS occur in northern Europe where the $T_{min,20}$ values can drop down to –50 °C in the Scandinavian Mountains (Fig. 2). In central Europe the cold extremes become warmer (from –25 to –15 °C) reaching a few degrees below zero in the southern part of the Iberian and Apennine Peninsulas. It is worth to note that typically the cold extremes have larger interannual variability comparing to the warm extremes (Kharin et al., 2007). Indeed, the scale parameter σ of the fitted GEV distribution for the annual T_{min} is almost twice as larger as the one for the annual T_{max} (not shown) that leads to wider confidence intervals for the estimated return values of T_{min} and consequently to less significant differences between the simulations and the E-OBS.

One distinct feature in the RCA3(ERA40) run is a warm bias (up to 12 °C) in northeastern Europe. We can expect, by analogy to T_{max}, that daily minimum temperature in winter is higher inside than outside of a forest and the simulated T_{min} is higher than that observed. We perform the corresponding analysis for the open-land $T_{min,20}$ from RCA35 driven by the ERA40 reanalysis. The warm bias in the grid box average $T_{min,20}$ is already reduced by 2–4 °C in RCA35, compared to RCA3 due to model improvements, but the reduction is almost doubled (4–8 °C) for the open-land $T_{min,20}$ (not shown). Hence, a part of the warm bias in $T_{min,20}$ in northeastern Europe is related to the fact that the E-OBS data set represents only the open-land temperature. At the same time biases in northeastern Europe are locally significant and have opposite sign among the simulations: positive in RCA3(ECHAM5, HadCM3 and CCSM3) and negative in RCA3(BCM, CNRM and IPSL). These differences between groups of simulations indicate the key role of the large-scale circulation defined by the driving GCMs. As a consequence of positive and negative biases in the individual simulations the ensemble mean shows almost no significant difference from the E-OBS data over this region.

Another typical feature in Fig. 2 is a cold bias over the Alps and the Scandinavian Mountains which is evident in all

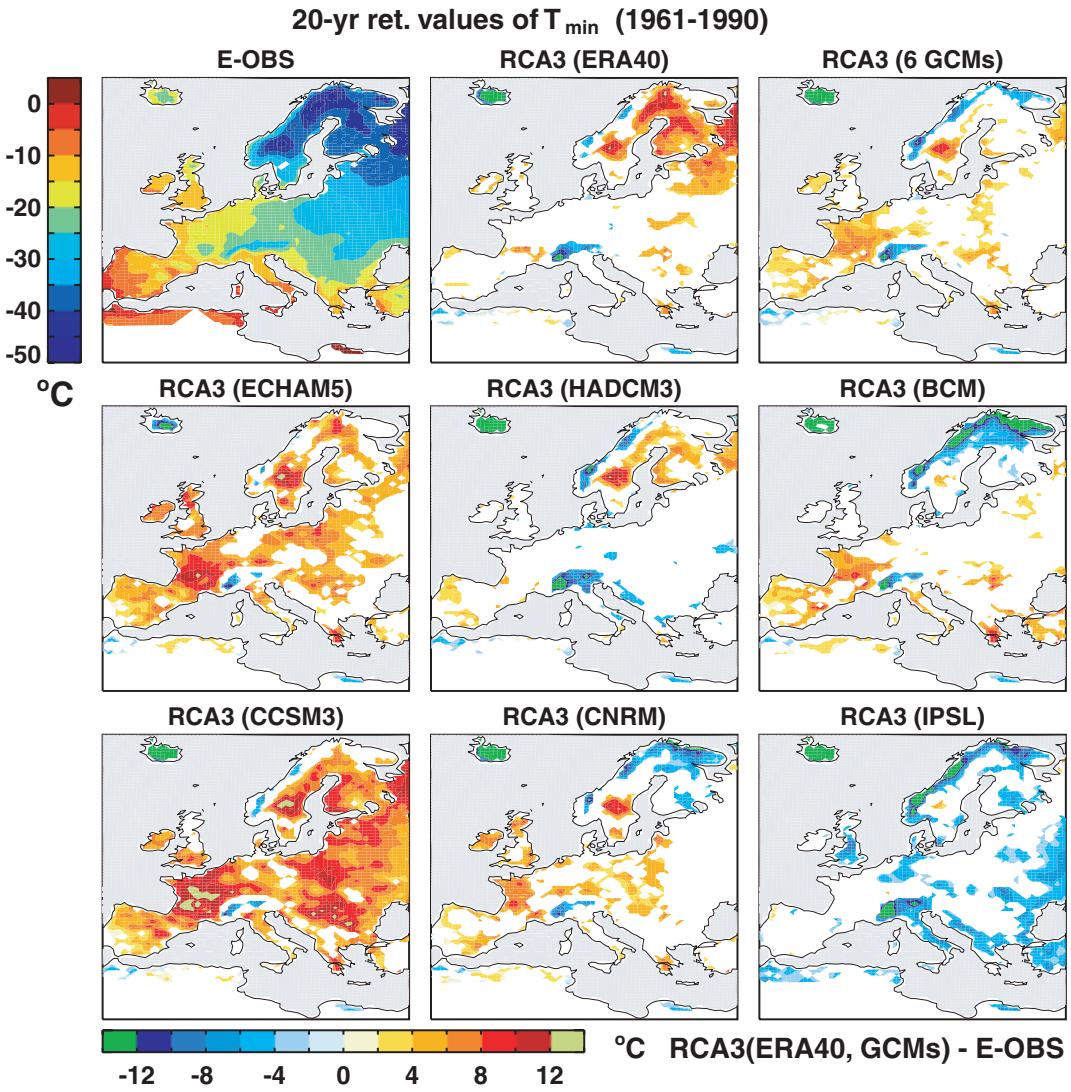

Fig. 2. The same as in Fig. 1 but for $T_{\mathrm{min},20}$.

simulations and, respectively, in the ensemble mean. A positive significant difference over France in the ensemble mean, which does not appear in the RCA3(ERA40) run, is originated from four simulations RCA3(ECHAM5, BCM, CCSM3 and CNRM) and especially from the CCSM3 and ECHAM5 driven runs where the warm bias is up to 12 °C and more in central France. There is a large geographical discrepancy between biases in seasonal mean winter temperature (Kjellström et al., 2011, fig. 2) and biases in cold extremes that do not typically coincide. For example, mean winter temperature in the above four simulations have the smallest differences from E-OBS over France. As for the $T_{\mathrm{max},20}$ the spatial patterns of the biases in $T_{\mathrm{min},20}$ in general follow those in the location parameter of the fitted GEV distribution (not shown). Also, the two warmest simulations—RCA3(ECHAM5) and RCA3(CCSM3) have a large negative bias in the scale parameter (about 80–100%) over France that in addition to the warmer location parameter results in less frequent cold extremes there. The large warm bias over most of Europe in the RCA3(CCSM3) simulation is related to a strengthened north–south pressure gradient in this driving GCM and consequently stronger zonal circulation that brings warm air masses from the Atlantic ocean to continental Europe in winter (Kjellström et al., 2011).

The results presented in Figs 1 and 2 show that the ensemble mean approach is really useful here since it substantially reduces large deviations of the individual members of the ensemble from the E-OBS. However, locally, large outliers of the individual simulations can become apparent also in the multi-model average resulting in biases which are not presented in the control RCA3(ERA40) simulation.

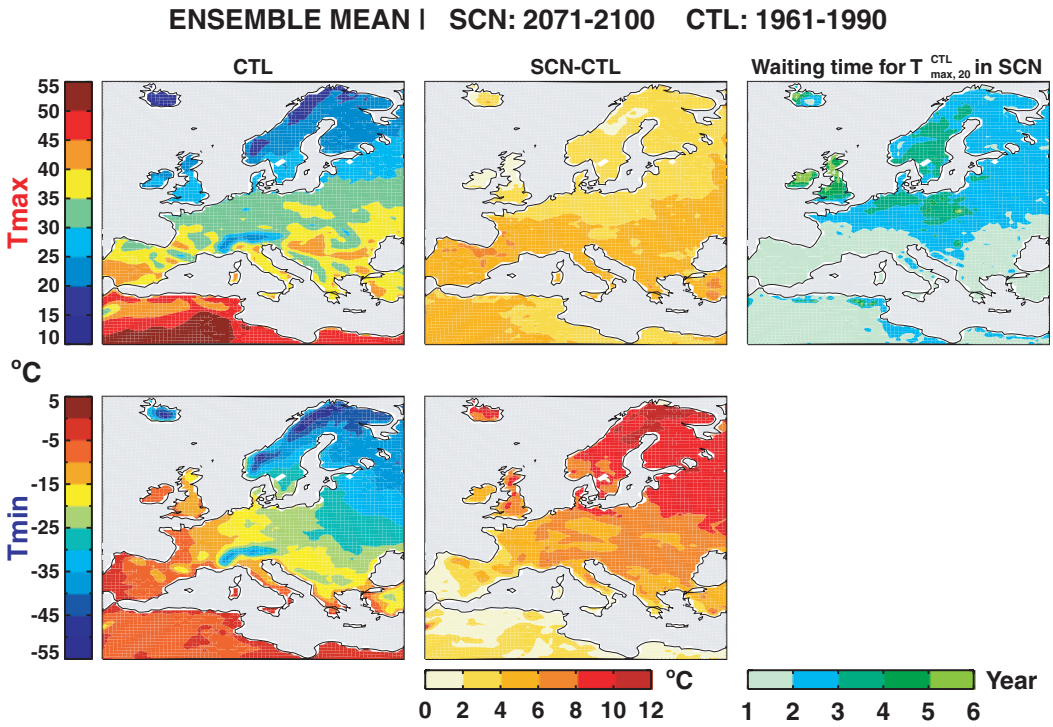

Fig. 3. Left-hand panels: the ensemble mean of (top panel) $T_{max,20}$ and (bottom panel) $T_{min,20}$ for 1961–1990 and (middle panel) the respective changes of $T_{max,20}$ and $T_{min,20}$ in 2071–2100 relative to 1961–1990 (°C). Only differences significant at the 10% significance level are shown. Right-hand panel: waiting times (years) of the 1961–1990 $T_{max,20}$ in 2071–2100.

3.2. *Changes in simulated temperature extremes*

Projections of the ensemble mean future changes in $T_{max,20}$ and $T_{min,20}$ are shown in Fig. 3. By the end of the century, the simulated high temperature extremes intensify over all Europe with an increase in $T_{max,20}$ of about 2–4 °C over northern Europe and 4–6 °C in southern and eastern Europe. Despite the large deviation among the simulations in the CTL period (Fig. 1) all six individual runs are quite consistent in representing the geographical distribution of the change with a typical difference of about 2 °C (not shown). The largest change in $T_{max,20}$ is found in the RCA3(ECHAM5) run where the increase in southern Europe reaches 10–12 °C. The spatial pattern of the projected future increase in $T_{max,20}$ closely follows that for seasonal mean summer temperature (Kjellström et al., 2011, fig. 6) and that for the location parameter (not shown) with almost the same magnitude. Although the projected changes in the location parameter are about the same among the simulations the corresponding changes in the scale parameter are much more noisy and differ from one driving model to another (not shown). In the ensemble mean the scale parameter shows an increase of 10–20% over France and 30–40% in the eastern part of Europe.

A comprehensive way to understand what a change of several °C in $T_{max,20}$ means is to estimate what becomes the waiting time or return period of the 1961–1990 $T_{max,20}$ in 2071–2100. From Fig. 3 it can be seen, that currently rare high temperatures become very common in the future. The simulated warm extremes that occur on average once in 20 yr (5% probability of occurring in any given year) in the CTL period may occur every year over southern Europe and every fifth year over Scandinavia in the SCN period.

The simulated cold extremes dramatically decline in the SCN period over northern Europe where $T_{min,20}$ becomes up to 12 °C warmer with respect to the CTL period (Fig. 3) and this warming signal can even reach 16 °C in individual runs. Such a strong decline in the cold extremes in high latitudes have been found in many studies with GCM and RCM simulations and attributed to reduced sea ice and snow cover under future global warming. (Kharin et al., 2007; Kjellström et al., 2007). Over central Europe $T_{min,20}$ gets higher by 4–8 °C and the smallest warming about 2 °C is found in the southwest part of the Iberian Peninsula and northern Africa. Again, as for $T_{max,20}$, all six simulations reproduce almost the same pattern of change with varying magnitude (not shown), although the estimated $T_{min,20}$ in the CTL period strongly differs among the members of the ensemble (Fig. 2). The spatial feature of the warming signal in the cold extremes completely repeats that in the winter mean temperature but the magnitude of the warming is almost doubled (Kjellström et al., 2011, fig. 4). The corresponding warm shift in the location parameter agrees well with the warming in $T_{min,20}$ and has very close magnitude (not shown).

Interannual variability of the cold extremes over central and southern Europe is reduced, the reduction in the scale parameter is 30–50%. In Scandinavia no significant changes in the interannual variability were found (not shown). Obviously, the strong warming in $T_{min,20}$ results in much smaller probability of recurrence of extremely cold events in the SCN period. The probability indeed becomes so small that the waiting time of the 1961–1990 $T_{min,20}$ values in 2071–2100, estimated by analogy to $T_{max,20}$, will be from several hundred years to infinity for the whole European domain (see also Kharin et al., 2007, fig. 9).

4. Precipitation extremes

4.1. Simulated precipitation extremes in the control period

Evaluation of the simulated precipitation extremes—$P_{max,20}$ for the 1961–1990 period is shown in Fig. 4. In the gridded observations the most heavy precipitation events, up to 100 mm d^{-1}, occur in mountain regions but with a seasonal difference. Such intense events are only a summer feature in the west Carpathian Mountains and only a winter feature in the mountain systems of the Iberian Peninsula, while they are evident in the Alps and the southwest part of the Scandinavian Mountains in both seasons. Outside of the mountain regions, spatial patterns of $P_{max,20}$ also differ between warm and cold seasons. In summer typical values of $P_{max,20}$ are about 30–50 mm d^{-1} over most of Europe with minimum (10–20 mm d^{-1}) in southern Italy, Greece and Turkey. Contrary to summer, a distinct winter feature is a north–south gradient in $P_{max,20}$ with the smallest values (10–20 mm d^{-1}) in eastern and northern Europe and the largest (30–50 mm d^{-1}) in southern Europe.

Spatial patterns of the biases in $P_{max,20}$ for all simulations driven by GCMs (not shown) as well for one driven by the ERA40 reanalysis (Fig. 4) show a complex structure since intense precipitation has a high degree of geographical variability defined by local topographical and meteorological conditions. The multimodel averaging slightly smoothes individual biases but the geographical pattern of the ensemble mean bias is still disperse (Fig. 4). In contrast to the temperature extremes (Figs 1 and 2) there is no large-scale dispersion in extreme precipitation between the members of the ensemble. All runs have some spotty tendency to underestimate $P_{max,20}$ in southern Europe and to overestimate it in northern Europe, although locally, the biases can be of the opposite sign and reaching several tens of percents (not shown). We should note that because of large interannual variability of extreme precipitation, the $P_{max,20}$ estimates have wide confidence intervals and only relative differences between the RCA3 simulations and the E-OBS data that are approximately larger than 30% for the individual simulations and than 20% for the ensemble mean are significant at the 10% significance level. Figure 4 shows all differences without separation to significant and insignificant to make the picture more readable.

Though the biases in Fig. 4 are very noisy there are some features which are common to all simulations. During summer the RCA3 simulations overestimate heavy precipitation over mountains and underestimate it over surrounding slopes. This detail is clearly seen for all mountain systems in southern Europe with alternating negative and positive differences from the Iberian to the Balkan Peninsula. In winter this pattern is less clear and in some areas absent, for example over the Pyrenees and Carpathian Mountains. A similar bias exists in the location parameter and slightly smaller in the scale parameter (not shown). An evaluation of the cloud fraction in RCA3 against satellite derived cloud products (Willén, 2008) has revealed that RCA3 has a large positive bias in the cloud fraction on top of the mountains and a negative bias on their slopes, most prominent on the leeside. These biases in the cloud fraction and precipitation extremes could be related to the overestimation of winds over the mountains in RCA (Georgelin et al., 2000) and excessive diffusion of humidity over steep orography. Both factors contribute to too much humidity on the top of mountain ranges that leads to enhancement of precipitation there and suppression of precipitation on the windward and lee slopes. For example, when the diffusion of moisture over steep orography is switched off in the Hadley Centre regional climate model—HadRM3 comparing to HadRM2 this leads to a removal of a spurious moisture source over high orography (Buonomo et al., 2007). Additional uncertainty in model evaluation in mountain regions is related to the gridded observations that may suffer from undersampling and systematic undercatch in high-elevation areas (Frei et al., 2003), which can also contribute to the difference.

Another common feature in all simulations is the overestimation of $P_{max,20}$ in northern Scandinavia that is particularly large in summer and has distinct counterparts in the location and scale parameters (not shown). There are only a few observational stations in this region (Haylock et al., 2008, fig. 1a) a fact that in combination with complex orography in northern Norway potentially may result in large uncertainties in the gridded precipitation data set and especially in extreme precipitation events. In order to validate heavy precipitation over this region we compare the $P_{max,20}$ estimates at five individual stations from the ECA data set in northern Norway with the nearest land grid points of RCA3 and E-OBS. There are also several stations in the northern part of the Kola Peninsula but only one station, Murmansk, is utilized because others have many gaps in daily precipitation data for the 1961–1990 period. As expected the $P_{max,20}$ gridded estimates from the E-OBS are reduced by 40–200% compared to the individual station estimates (not shown). In contrast simulated $P_{max,20}$ is overestimated by 40–100% at all grid points in northern Norway but in good agreement at the Murmansk station. Here we cannot attribute exactly a source of the difference between the E-OBS and RCA3 as both the RCA3 formulation and the uncertainties in the E-OBS potentially contribute to the difference. One possible speculation which can explain a part of the difference is that almost all station in northern Norway are

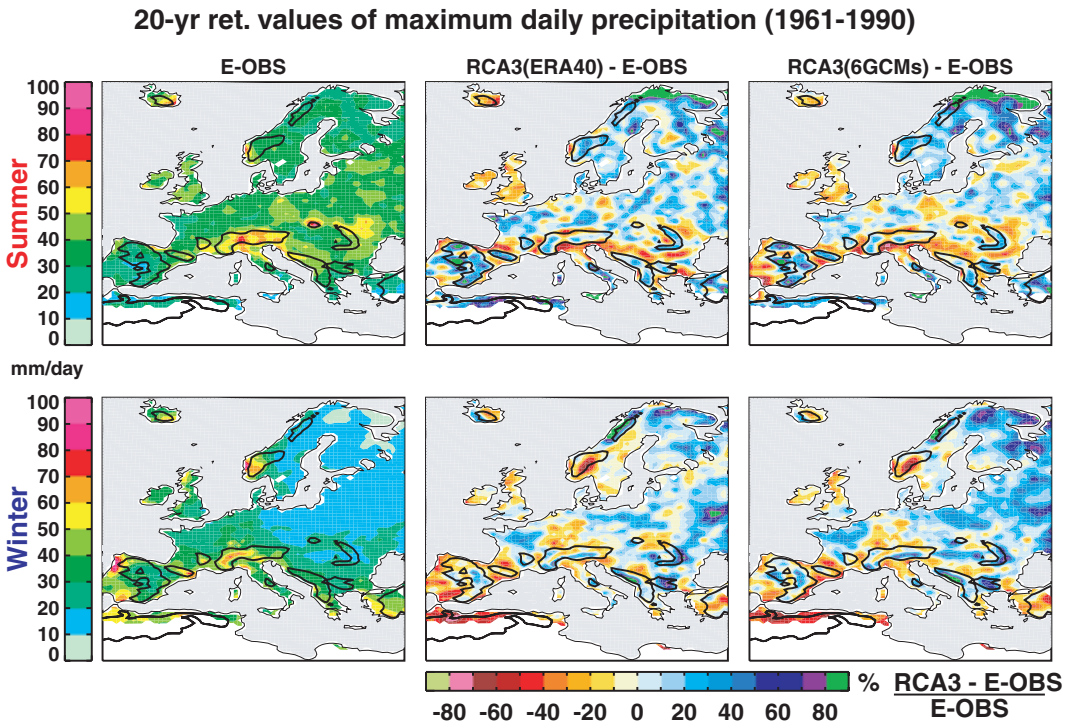

Fig. 4. (top panel) The summer and (bottom panel) winter $P_{\max,20}$ estimated from (left-hand panel) the E-OBS data (mm d^{-1}) and biases of $P_{\max,20}$ estimated from the RCA30 simulations driven by (middle panel) the ERA40 reanalysis and (right-hand panel) by six different GCMs in terms of their ensemble mean with respect to the E-OBS (1961–1990) (%). All differences which approximately lie outside of ±30% for the ERA3(ERA40) run and of ±20% for the ensemble mean are significant at the 10% significance level. Thick black lines are 700 m contours of RCA3 topography.

located at low elevations (10–150 m) while the nearest land grid points of RCA are located at elevation of several hundred metres that results in more intense simulated precipitation than the observed or gridded ones. At the same time for the northern part of the Kola Peninsula which is more plain compared to northern Norway, corresponding altitude differences are smaller and simulated $P_{\max,20}$ is in better agreement with observed $P_{\max,20}$. Another possible source of the bias is that this region is located just south of the boundary relaxation zone where accumulation of humidity (no transport outside the RCA3 domain) is possible.

Overall, in a large part of central Europe and Scandinavia the difference between the simulated and gridded $P_{\max,20}$ falls within 20–30% that is not significant at the 10% level hence RCA performance is good there.

4.2. *Changes in simulated precipitation extremes*

The projected changes in extreme precipitation for the ensemble are shown in Fig. 5 for summer and in Fig. 6 for winter. We do not separate between statistically significant and insignificant changes here by showing only the significant ones because for individual simulations only scattered colour spots left in this case that completely destroys visual perception of the results. Instead, we note that only the changes which approximately lie outside of ±30% for the individual members and of ±10% for the ensemble mean are statistically significant at the 10% significance level. The ensemble mean difference is calculated here as a difference between two ensemble means (SCN and CTL) that results in the smaller insignificant interval (±10%) comparing to the corresponding one (±20%) for Fig. 4 where the subtrahend (E-OBS) is an individual estimate with the wider confidence intervals.

In summer all individual projections have complex patterns with mixed small-scale negative and positive changes (Fig. 5). The RCA3(HadCM3) and RCA3(IPSL) driven runs show the least dispersed signal and the most prominent intensification of heavy precipitation up to 60% and more almost for all Europe. The other four simulations project smaller and more heterogeneous changes in $P_{\max,20}$ and just a few local spots are significant. Although, on average, there is a somewhat large-scale tendency to an increase in heavy precipitation in northern Europe and a decrease in southern Europe, on regional scales there is almost no area where all driving models agree even in sign. The ensemble mean smoothes the diverse individual projections resulting in a more homogeneous pattern with a 10–30% significant increase of $P_{\max,20}$ over Scandinavia and some parts of Poland and the Baltic countries and a 10–40% significant decrease over the southwestern Iberian Peninsula. In other regions in Europe the ensemble mean changes in $P_{\max,20}$ are within ±10% and not significant. The changes in the location parameter mostly

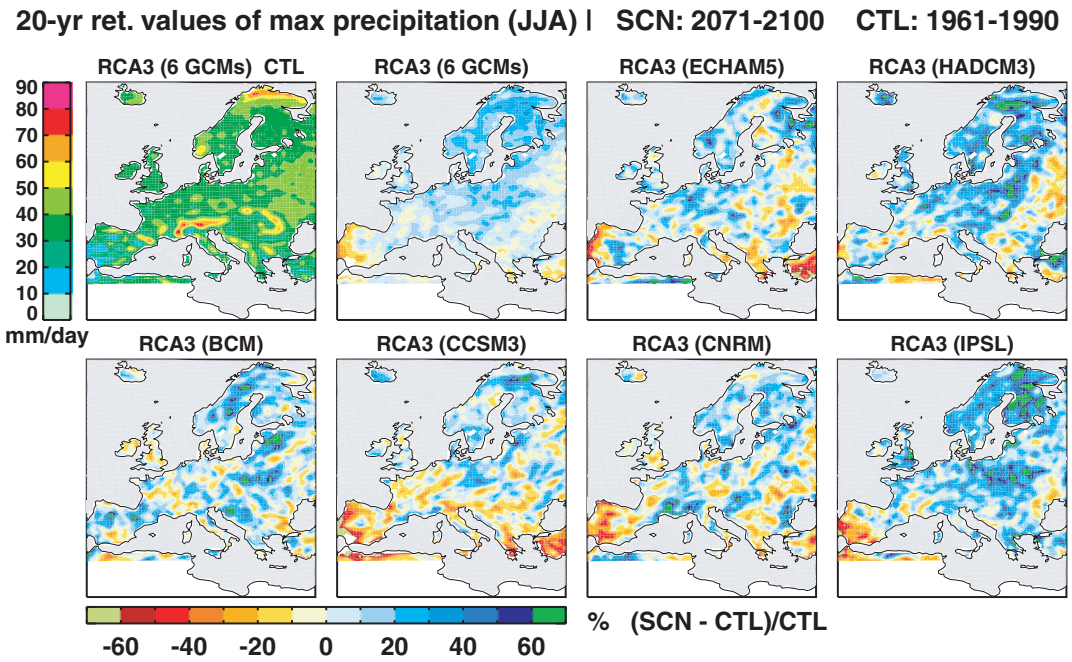

Fig. 5. (top, right-hand panel) The ensemble mean $P_{\max,20}$ in summer for 1961–1990 (mm d^{-1}) and the projected changes in $P_{\max,20}$ (%) for six individual simulations and their ensemble mean. All changes which approximately lie outside of ±30% for the individual simulations and of ±10% for the ensemble mean are significant at the 10% significance level.

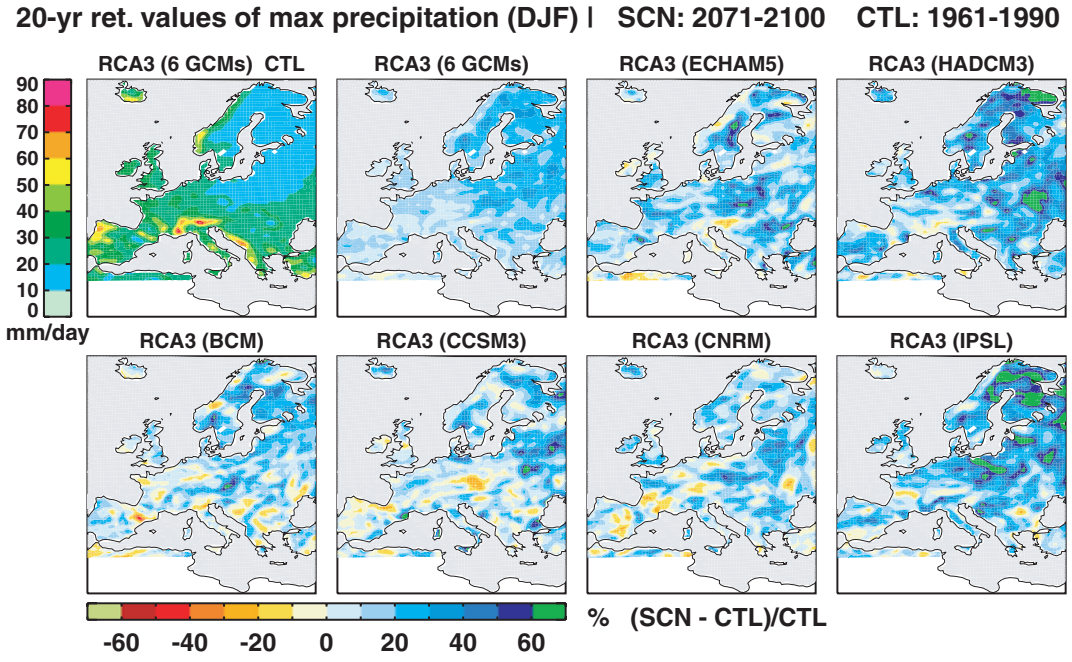

Fig. 6. The same as in Fig. 5 but for winter.

define the geographical distribution of the changes in $P_{\max,20}$ and regionally the magnitude of the change can be amplified by an additional increase in the scale parameter that is special feature of the RCA3(HadCM3) and RCA3(IPSL) runs (not shown).

The simulated wintertime precipitation extremes increase in SCN over a considerable part of Europe (Fig. 6) and have more consistent geographical patterns of the change among the simulations compared to summer (Fig. 5). Again, the HadCM3 and IPSL driven runs which project the largest increase in

summertime $P_{max,20}$ show the largest increase also in wintertime $P_{max,20}$ with only a few places with a decrease in $P_{max,20}$ The ensemble average shows intensification of precipitation extremes over all Europe (Fig. 6) with the most prominent significant increase (20–40%) in Scandinavia and northeastern Europe. The magnitude of the projected changes decreases southand westward and remains statistically significant above 10% in some regions, for example, Italy, northern France and parts of the Iberian and Balkan Peninsulas. Large-scale patterns of the $P_{max,20}$ change mainly follow their counterparts in the location parameter with some exceptions in regions where the scale parameter changes are large that additionally suppress or enhance the projected $P_{max,20}$ (not shown).

The increase of $P_{max,20}$ in the simulated future climate that is evident from Figs 5 and 6 means that precipitation extremes will become more frequent. Figure 7 displays what the recurrence time for the CTL period 20-yr return values for precipitation extremes becomes at the end of the 21st century. The recurrence time reduces from 20 to 6–10 yr over northern and some parts of central Europe in summer (Fig. 7). The reduction to 10 yr and less approximately coincides with the ensemble mean changes in $P_{max,20}$ that are larger than 10% (see Figs 5 and 6) and is considered as statistically significant. In winter the recurrence time reduces even more down to 2–4 yr locally in Scandinavia and the significant reduction covers a much larger domain.

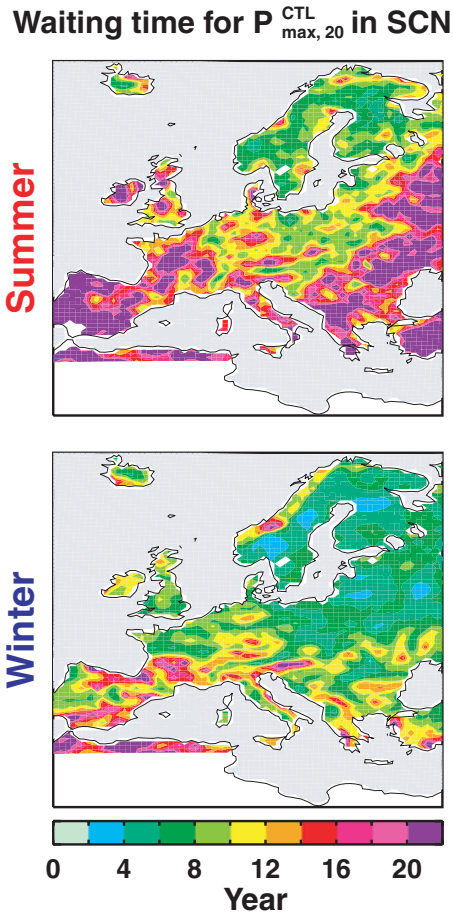

Fig. 7. Waiting times (years) of the 1961–1990 $P_{max,20}$ in 2071–2100 for (top panel) summer and (bottom panel) winter.

5. Wind extremes

5.1. *Changes in simulated wind extremes*

The ensemble mean $W_{max,20}$ for the CTL period ranges from 18 to 50 m s^{-1} over the model domain with minimum in northern and eastern Europe and maximum over the Northeast Atlantic (Fig. 8). All individual simulations show a similar pattern defined basically by the land and sea distribution but values can locally differ by 10 m s^{-1} and more (not shown). Unfortunately, as we have already mentioned in the introduction, there is no suitable observational database to evaluate the simulated $W_{max,20}$.

The projected changes in $W_{max,20}$ in the SCN period show a wide spread among the six simulations (Fig. 8). In the Northeast Atlantic, where the largest wind gusts are simulated, the changes vary from −6 to 6 m s^{-1} in different runs without any coherent pattern. This results in scattered statistically significant spots of both signs in the ensemble average with a typical absolute values of 1 m s^{-1}. The same picture is characteristic for the continent where the ensemble average shows localized significant increases or decreases on the average of 1 m s^{-1} in $W_{max,20}$. We can note some tendency of strengthening of extreme gust winds approximately north of 45°N and weakening south of it in the ensemble mean. However, over northern France, Belgium and Netherlands, where the strengthening is evident in the ensemble mean, three simulations RCA3 (HadCM3, BCM and CNRM) show an increase in $W_{max,20}$ while the other three show a decrease or no change. The climate change signal is more robust over the Baltic Sea in this sense: all simulation with the exception of the CNRM driven one project strengthening of extreme gust winds there. Tendencies to weakening of extreme gust winds south of 45°N exist in all runs but again regional-scale patterns are very different. In order to test stability of the ensemble mean results we have generated six new ensembles of five member excepting each time one simulation. Both tendencies, an increase in $W_{max,20}$ over the Baltic Sea and a decrease in south of 45°N are preserved in all new ensembles although, local details can strongly differ (not shown). We can conclude that including new members to the present ensemble would most likely modify the structure of regional projections in the ensemble mean results for $W_{max,20}$.

6. Summary and conclusions

An ensemble of regional climate simulations is utilized to evaluate statistics of temperature, precipitation and wind extremes over Europe for the control (1961–1990) and a possible

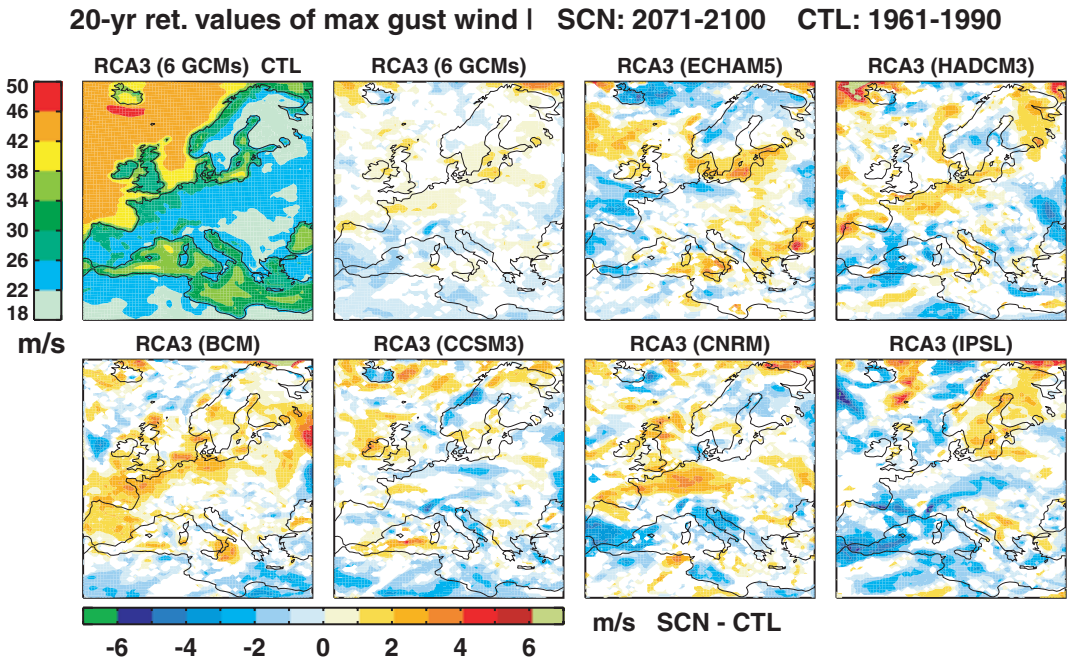

Fig. 8. (top, left-hand panel) The ensemble mean $W_{max,20}$ for 1961–1990 (m s^{-1}) and the projected changes in $W_{max,20}$ for six individual simulations and their ensemble mean. Only the changes significant at the 10% significance level are shown.

future (2071–2100) climate under the SRES A1B emission scenario. The ensemble consists of six members and is based on a regional climate model—RCA3 that is driven by six different GCMs (ECHAM5, CCSM3, HadCM3, CNRM, BCM and IPSL). Extreme events are expressed in terms of the 20-yr return values that are estimated by fitting the generalised extreme value distribution to annual maximum/minimum daily temperature at 2 m, maximum summer/winter accumulated daily precipitation and annual maximum of daily maximum gust wind. For the 1961–1990 control period the performance of the ensemble mean and its individual members in simulating temperature and precipitations extremes is evaluated against a daily high-resolution gridded observational data set for Europe—E-OBS. Absence of a consistent gridded data set for gust wind precludes us from analogous evaluation of wind extremes. The projected future changes in statistics of temperature, precipitation and gust wind extremes in 2071–2100 relative to the reference period 1961–1990 are determined and a degree of their dependency on driving GCMs is investigated. The main results of the study are summarized as follow.

6.1. Temperature extremes

For the control period—CTL all simulations strongly underestimate warm extremes (about 10 °C) over Scandinavia comparing to the gridded observations. This negative bias is related to the fact that Scandinavia has a large fraction of forest and the observations represent only the open-land temperature while the simulated temperature is individually calculated for forest and open land and then averaged. A part of the underestimation of cold extremes (up to 12 °C) over northeastern Europe in the RCA3(ERA40) simulation is also related to the open-land issue but errors in the large-scale circulation from the driving global models strongly dominate biases over this region that are of opposite sign among the simulations driven by GCMs. A common positive bias for the simulated cold extremes is found over the Alps and Scandinavian Mountains and reaches more than 12 °C in individual simulations. In central and southern Europe a difference among simulations driven by different GCMs for both warm and cold extremes can be of opposite sign and reaches 20 °C and more. On the average spatial patterns of the biases in the 20-yr return values follow the corresponding ones in the location parameter of the fitted GEV distribution. In addition, the largest absolute deviations from the observations are attributed to the simulations with large biases in the scale parameter that means under- or overestimation of interannual variability of temperature extremes. The ensemble mean approach substantially reduces individual biases and is in good agreement with the control RCA3(ERA40) run. Despite the large deviations among simulations in the CTL period all six simulations show quite consistent geographical patterns of the projected future changes in temperature extremes that differ in magnitude. The ensemble mean warm extremes intensify over all Europe with an increase of about 2–4 °C over northern Europe and 4–6 °C in southern Europe while the cold ones becomes up to 12 °C warmer in northern Europe and 2–6 °C warmer in central and southern

Europe. Interannual variability (the scale parameter) increases by 10–20% over France and by 30–40% in eastern Europe for warm extremes and decreases by 30–50% in central and southern Europe for cold extremes. The warm temperature extremes that occur once in 20 yr in CTL may occur every year over southern Europe and every fifth year over Scandinavia in SCN while cold extremes may almost disappear.

6.2. *Precipitation extremes*

Spatial patterns of biases in precipitation extremes in CTL for all individual simulation have a complex, spotty structure that is only slightly smoothed in the ensemble mean, though some details are evident in all simulations. In summer the simulated precipitation extremes are overestimated over mountains and underestimated over surroundings slopes. This feature is most likely related to the too strong winds and excessive diffusion of humidity over steep orography in the RCA3 formulation, though undersampling and systematic undercatch over high-elevation areas in the observations can also play a role. All simulations show too intense precipitation extremes in northern Scandinavia, specially in summer. A source of this bias cannot be exactly attributed since this region is located just south of the boundary relaxation zone of the RCA3 domain (accumulation of humidity is possible) and the gridded observation may suffer from just a few observational stations there. In both winter and summer, over a large part of central Europe and Scandinavia the relative difference between the simulated and observed precipitation extremes is within the $\pm 30\%$ interval. The projected future changes in summertime extreme precipitation for the individual simulations show mixed small-scale changes with, on average, a tendency to an increase in northern and a decrease in southern Europe. The ensemble mean 20-yr return levels significantly increase by 10–30% in Scandinavia, Poland and the Baltic countries and decrease by 10–40% over southwestern parts of the Iberian Peninsula while no significant changes (larger than 10%) are found over other regions. In winter the spatial patterns of the change in heavy precipitation are more consistent among the individual simulations showing intensification of precipitation extremes over most of Europe. The ensemble average, however, shows a significant large-scale increase by 20–40% only in Scandinavia and northeastern Europe and several local significant intensifications (above 10%), for example, in Italy, northern France and a part of Iberian and Balkan Peninsulas. The recurrence time of intense precipitation reduces from 20 yr in CTL to 6–10 yr in SCN over northern and some parts of central Europe in summer and even more to 2–4 yr locally in Scandinavia in winter.

6.3. *Wind extremes*

All simulations show a similar large-scale pattern of wind extremes in CTL that is defined by the land and sea distribution with the largest ensemble mean 20-yr return values (42–50 m s^{-1}) in the North East Atlantic and the smallest ones (18–22 m s^{-1}) in northern and eastern Europe. At the same time the individual runs can locally differ by 10 m s^{-1} and more. The projected changes in wind extremes have a very wide, heterogeneous spread without any coherent pattern among the six ensemble members. As result the ensemble average change is scattered significant spots of both signs with a typical absolute magnitude of 1 m s^{-1}. There is a weak spotty tendency of strengthening of wind extremes approximately north of 45°N and weakening south of it but locally the individual simulations can project different signs of the change. The more robust strengthening of gust winds is found over the Baltic Sea where only one simulation of six shows no changes. Excluding one simulation from the ensemble mean, on average, preserves the tendencies but again the local details can be strongly different.

In the control period 1961–1990, a degree of dependency of all simulated extremes on a driving GCM is very large since differences among the individual simulations can reach 20 °C for temperature extremes, several tens of percents for precipitation extremes and 10 m s^{-1} for wind extremes. Nevertheless, the projected future changes in temperature extremes show coherent spatial patterns among the simulations with different magnitude. The corresponding changes in precipitation extremes have much less consistent geographical patterns with many small-scale local details varying in magnitude and sign, though a common tendency can be identified. The projected future changes in wind extremes are strongly different among the simulations driven by different GCMs and we can hardly say that there is any common tendency. We can conclude that for the present ensemble of regional climate simulations the future changes in temperature extremes are more robust to a choice of a driving GCM than ones in precipitation extremes while we have almost no confidence on the projected changes in wind extremes.

7. Acknowledgments

Part of this work has been performed under the Swedish Mistra-SWECIA programme. We acknowledge the E-OBS data set from the EU-FP6 project ENSEMBLES (http://www.ensembles-eu.org) and the data providers in the ECA&D project (http://eca.knmi.nl). The institutes providing the global model data used as boundary conditions are kindly acknowledged. All model simulations were made on the climate computing resource Tornado funded with a grant from the Knut and Alice Wallenberg foundation. We also thank two anonymous reviewers for their helpful comments.

References

Beniston, M., Stephenson, D. B., Christensen, O. B., Ferro, C. A. T., Frei, C. and co-authors. 2007. Future extreme events in European climate: an exploration of regional climate model projections. *Clim. Change* **81**, 71–95, doi:10.1007/s10584-006-9226-z.

Brasseur, O. 2001. Development and application of a physical approach to estimating wind gusts. *Mon. Wea. Rev.* **129**, 5–25.

Buonomo, E., Jones, R., Huntingford, C. and Hannaford, J. 2007. On the robustness of changes in extreme precipitation over Europe from two high resolution climate change simulations. *J. R. Meteor. Soc.* **133**, 65–81.

Christensen, J. H. and Christensen, O. B. 2003. Severe summertime flooding in Europe. *Nature* **421**, 805–806.

Christensen, J. H., Hewitson, B., Busuioc, A., Chen, A., Gao, X. and co-authors. 2007. Regional climate projections. In: *Climate Change 2007: The Physical Science Basis. Contribution of Working Group I to the Fourth Assessment Report of the Intergovernmental Panel on Climate Change* (eds S. Solomon, D. Qin, M. Manning, Z. Chen, M. Marquis and co-editors). Cambridge University Press, Cambridge, United Kingdom and New York, NY, USA.

Coles, S. 2001. *An Introduction to Statistical Modeling of Extreme Value*. Springer-Verlag, Berlin and Heidelberg, 208.

Della-Marta, P. M., Mathis, H., Frei, C., Liniger, M. A. and Appenzeller, C. 2007. Extreme wind storms over Europe: statistical analyses of ERA-40. *Arbeitsberichte der MeteoSchweiz* **216**, 79.

Déqué M., Rowell, D., Lüthi, D., Giorgi, F., Christensen, J. and co-authors. 2007. An inter-comparison of regional climate models for Europe: model performance in present-day climate. *Clim. Change* **81**, 53–70, doi:10.1007/s10584-006-9228-x.

Fischer, E. M. and Schär, C. 2009. Future changes in daily summer temperature variability: driving processes and role for temperature extremes. *Clim. Dyn.* **32**, doi:10.1007/s00382-008-0473-8.

Frei, C., Christensen, J. H., Déqué, M., Jacob, D., Jones, R. G. and Vidale, P. L. 2003. Daily precipitation statistics in regional climate models: evaluation and intercomparison for the European Alps. *J. Geophys. Res.* **108**(D3), 4124, doi:10.1029/2002JD002287.

Frei, C., Schöll, R., Fukutome, S., Schmidli, J. and Vidale, P. L. 2006. Future change of precipitation extremes in Europe: intercomparison of scenarios from regional climate models. *J. Geophys. Res.* **111**, D06105, doi:10.1029/2005JD005965.

Georgelin, M., Bougeault, P., Black, T., Brzovic, N., Buzzi, A. and co-authors. 2000. The second COMPARE exercise: a model intercomparison using a case of a typical mesoscale orographic flow, the PYREX IOP3. *Q. J. R. Meteor. Soc.* **126**, 991–1030.

Goubanova, K. and Li, L. 2007. Extremes in temperature and precipitation around the Mediterranean basin in an ensemble of future climate scenario simulations. *Glob. Planet. Change* **57**, 27–42.

Gutowski, W. J., Hegerl, G. C., Holland, G. J., Knutson, T. R., Mearns, L. O. and co-authors. 2008. Causes of observed changes in extremes and projections of future changes. In: *Weather and Climate Extremes in a Changing Climate.Regions of Focus: North America, Hawaii, Caribbean, and U.S. Pacific Islands*. (eds T. R. Karl, G. A. Meehl, C. D. Miller, S. J. Hassol, A. M. Waple and co-editors). A Report by the U.S. Climate Change Science Program and the Subcommittee on Global Change Research, Washington, DC.

Häggmark, L., Ivarsson, K.-I., Gollvik, S. and Olofsson, P.-O. 2000. Mesan, an operational mesoscale analysis system. *Tellus* **52A**, 2–20.

Haylock, M. R., Hofstra, N., Klein Tank, A. M. G., Klok, E. J., Jones, P. D. and co-authors. 2008. European daily high-resolution gridded data set of surface temperature and precipitation for 1950–2006. *J. Geophys. Res.* **113**, D20119, doi:10.1029/2008JD010201.

Hosking, J. R. M. 1990. L-moments: analysis and estimation of distributions using linear combination of order statistics. *J. Roy. Stat. Soc.* **52B**, 105–124.

Hosking, J. R. M., Wallis, J. R. and Wood, E. F. 1985. Estimation of the generalized extreme-value distribution by the method of probability weighted moments. *Technometrics* **27**, 251–261.

Kharin, V. V. and Zwiers, F. W. 2000. Changes in extremes in am ensemble of transient simulations with a coupled atmosphere-ocean GCM. *J. Clim.* **13**, 3760–3788.

Kharin, V. V. and Zwiers, F. W. 2004. Estimating extremes in transient climate change simulations. *J. Clim.* **18**, 1156–1173.

Kharin, V. V., Zwiers F. W., Zhang X. and Hegerl, G. C. 2007. Changes in temperature and precipitation extremes in the IPCC ensemble of global coupled model simulations. *J. Clim.* **20**, 1419–1444.

Kjellström, E. 2004. Recent and future signatures of climate change in Europe. *Ambio* **33**, 193–198.

Kjellström, E., Bärring, L., Hansson, U., Jones, C., Samuelsson, P. and co-authors. 2005. A 140-year simulation of European climate with the new version of the Rossby Centre regional atmospheric climate model (RCA3). *SMHI Reports Meteorology and Climatology* Volume 108, SMHI, SE-60176 Norrköping, Sweden, 54.

Kjellström, E., Bärring, L., Jacob, D., Jones, R., Lenderink, G. and co-authors. 2007. Modelling daily temperature extremes: recent climate and future changes over Europe. *Clim. Change* **81**, 249–265.

Kjellström, E., Nikulin, G., Hansson, U., Strandberg, G. and Ullerstig, A. 2011. 21st century changes in the European climate: uncertainties derived from an ensemble of regional climate model simulations. *Tellus* **63A**, 24–40.

Klein Tank, A. M. G., Wijngaard, J. B., Können, G. P., Böhm, R., Demarée, G. and co-authors. 2002. Daily dataset of 20th-century surface air temperature and precipitation series for the European Climate Assessment. *Int. J. of Climatol.* **22**, 1441–1453.

Kunkel, K. E., Bromirski, P. D., Brooks, H. E., Cavazos, T., Douglas, A. V. and co-authors. 2008. Observed Changes in Weather and Climate Extremes. In: *Weather and Climate Extremes in a Changing Climate. Regions of Focus: North America, Hawaii, Caribbean, and U.S. Pacific Islands*. (eds T. R. Karl, G. A. Meehl, C. D. Miller, S. J. Hassol, A. M. Waple and co-editors). A Report by the U.S. Climate Change Science Program and the Subcommittee on Global Change Research, Washington, DC.

Kyselý, J. 2002. Comparison of extremes in GCM-simulated, downscaled and observed central-European temperature series. *Clim. Res.* **20**, 211–222.

Leckebusch, G. C., Koffi, B., Ulbrich, U., Pinto, J., Spangehl, T. and co-authors. 2006. Analysis of frequency and intensity of winter storm events in Europe on synoptic and regional scales from a multi-model perspective. *Clim. Res.* **31**, 59–74.

Nakićenović, N., Alcamo, J., Davis, G., de Vries, B., Fenhann, J. and co-authors. 2000. *IPCC Special Report on Emissions Scenarios*. Cambridge University Press, New York, 599.

Nordström, M. 2005. *Estimation of Gusty Winds in RCA*. Master Thesis, The Department of Earth Sciences, Uppsala University. ISSN 1650–6553 Nr. 101. 42 pp. (http://www.geo.uu.se/luva/exarb/2005/Maria_Nordstrom.pdf).

Räisänen, J., Hansson, U., Ullerstig, A., Döscher, R., Graham, L. P. and co-authors. 2003. GCM driven simulations of recent and future climate with the Rossby Centre coupled atmosphere—Baltic Sea regional climate model RCAO. *Reports Meteorology and Climatology*

Volume 101, Swedish Meteorological and Hydrological Institute, SE-601 76 Norrköping, Sweden, 61.

Räisänen, J., Hansson, U., Ullerstig, A., Döscher, R., Graham, L. P. and co-authors. 2004. European climate in the late twenty-first century: regional simulations with two driving global models and two forcing scenarios. *Clim. Dyn.* **22**, 13–31.

Rockel, B. and Woth, K. 2007. Extremes of near surface wind speed over Europe and their future changes as estimated from an ensemble of RCM simulations. *Clim. Change* **81**, 267–280.

Rowell, D. P. 2005. A scenario of European climate change for the late twenty-first century: seasonal means and interannual variability. *Clim. Dyn.* **25**, 837–849.

Samuelsson, P., Gollvik, S. and Ullerstig, A. 2006. The land-surface scheme of the Rossby Centre regional atmospheric climate model (RCA3). SMHI Meteorologi No. 122. 25.

Samuelsson P., Jones, C., Willén, U., Gollvik, S., Hansson, U. and co-authors. 2011. The Rossby Centre Regional Climate Model RCA3: model description and performance. *Tellus* **63A**, 4–23.

Schär C, Vidale P. L, Lüthi D., Frei C., Häberli C. and co-authors. 2004. The role of increasing temperature variability for European summer heat waves. *Nature*, **427**, 332–336.

Trenberth, K. E., Jones, P. D., Ambenje, P., Bojariu, R., Easterling, D. and co-authors. 2007. Observations: surface and atmospheric climate change. In: *Climate Change 2007: The Physical Science Basis. Contribution of Working Group I to the Fourth Assessment Report of the Intergovernmental Panel on Climate Change* (eds S. Solomon, D. Qin, M. Manning, Z. Chen, M. Marquis and co-editors). Cambridge University Press, Cambridge, United Kingdom and New York, NY, USA.

von Storch, H. and Zwiers, F. W. 1999. *Statistical Analysis in Climate Research*. Cambridge University Press, Cambridge, 484.

Willén, U. 2008. Preliminary use of CM-SAF cloud and radiation products for evaluation of regional climate simulations. *Reports Meteorology and Climatology* Volume 131, Swedish Meteorological and Hydrological Institute, SE-601 76 Norrköping, Sweden, 48.